

Experimental Bond Dissociation Energies of Benzylpyridinium Thermometer Ions determined by Threshold-CID and RRKM modeling.

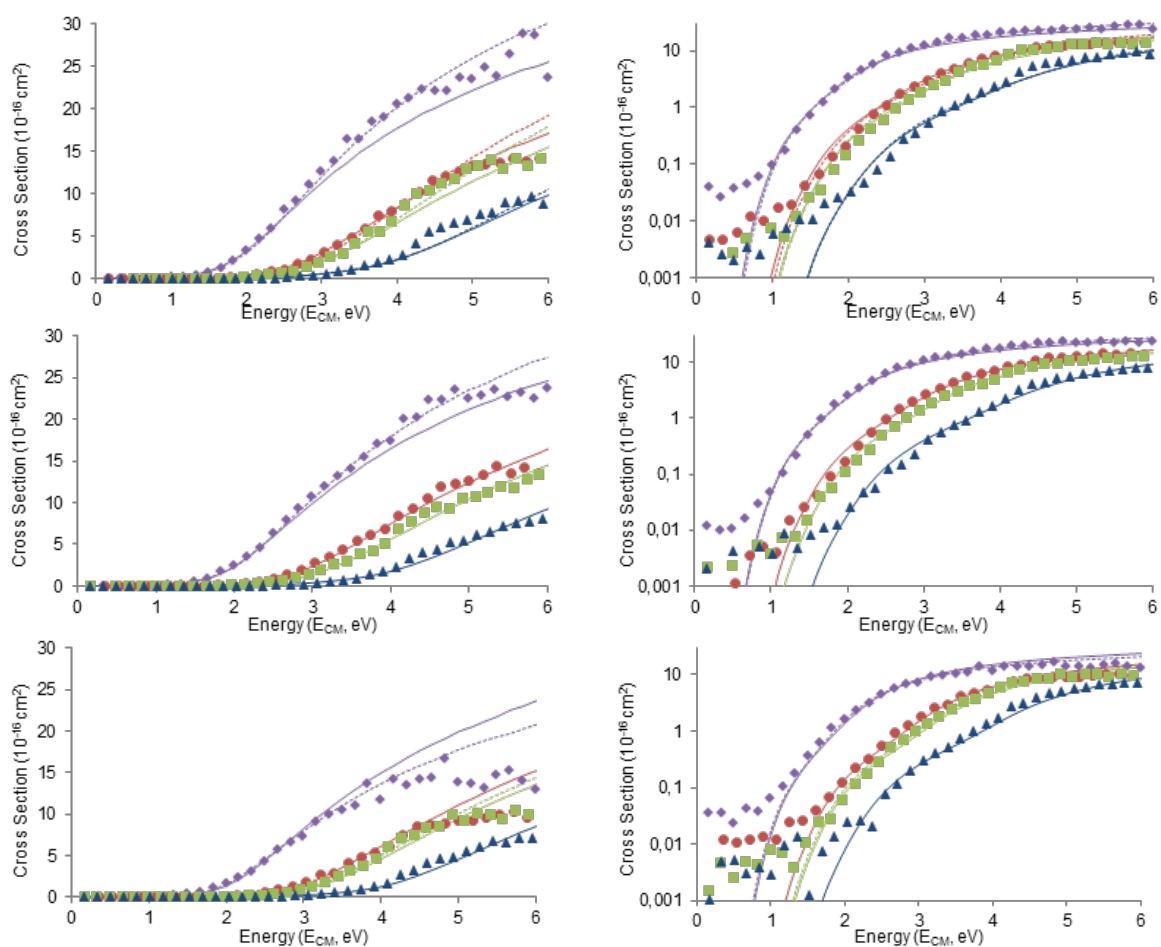
David Gatineau,^{1,3} Antony Memboeuf,² Anne Milet,³ Richard B. Cole,¹ H elo ise Dossmann,¹ Yves Gimbert,³ Denis Lesage^{1*}

1) Sorbonne Universit es, UPMC Univ. Paris 06 and CNRS, IPCM (UMR 8232), F-75252 Paris Cedex05, France

2) Univ. Bretagne Occidentale and CNRS, CEMCA (UMR 6521), F-29238 Brest, France

3) Univ. Grenoble Alpes and CNRS, DCM (UMR 5250), F-38000 Grenoble, France

1. Experimental data and MassKinetics modeling



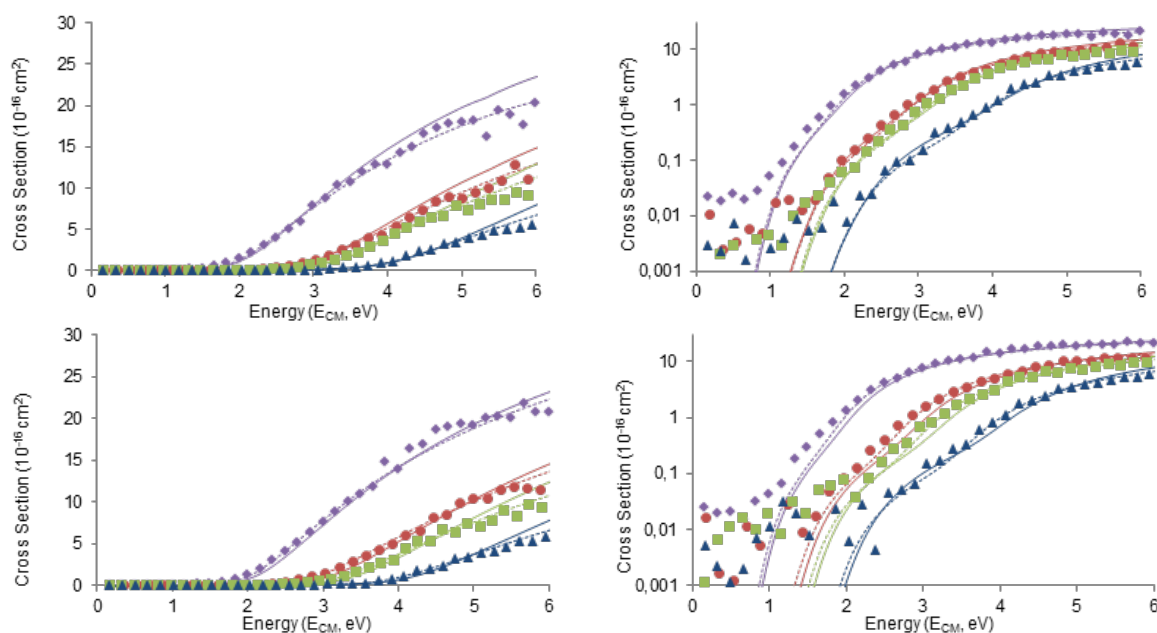
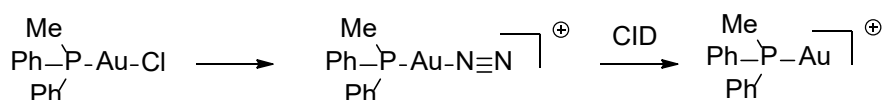


Figure S1. Experimental cross sections for TCID of pOMe **1** (purple diamonds), pMe **2** (red circles), pCl **3** (green squares) and pCN **4** (blue triangles) with Ar as a function of center-of-mass energy at 1.48×10^{-4} , 1.23×10^{-4} , 8.3×10^{-5} , 6.5×10^{-5} , and 3.8×10^{-5} mbar (from the top to the bottom). The dashed lines correspond to variable efficiency curves. The solid lines correspond to a fixed efficiency of 0.18. Normal (left) and logarithmic (right) scales are shown.

2. Pressure calibration using an all-metal regulating valve UDV 040

$[\text{MePh}_2\text{PAuN}_2]^+$ ions were formed from $[\text{MePh}_2\text{PAuCl}]$ solution in methanol ($10 \mu\text{g/mL}$) in the Z-spray ESI source of the homemade in-house modified Quattro II triple quadrupole (Micromass, Manchester, UK) with a flow rate of $200 \mu\text{L/hr}$, capillary voltage 3.5 kV , cone voltage 20 V , extractor 2 V , source block/drying gas temperature $100/100 \text{ }^\circ\text{C}$. After collision in h2 with Ar or Xe, $[\text{MePh}_2\text{PAuN}_2]^+$ complexes seem particularly unstable (Scheme S1). We used the dissociation of this complex to calibrate the pressure.



Scheme S1. Formation of $[\text{MePh}_2\text{PAuN}_2]^+$ followed by collision induced dissociation.

At constant collision voltage (20 V), product ion intensities ($I_P/(I_P + I_R)$ where I_P is the product ion abundance and I_R is reactant ion abundance) can be represented as a function of number of turns of the micrometric valve. Using the pressure read on the gauge at 2 turns of the micrometric valve as a pressure of reference ($P = 3.2 \times 10^{-5}$ mbar for Ar and $P = 7.5 \times 10^{-6}$ mbar for Xe), two calibration curves of the pressure as a function of number of turns of valve were obtained using the fit of the data with *MassKinetics* software (figure S2). The following parameters were used: critical energy = 0.3 eV , initial internal energy distribution of 300 K , frequency models calculated at BMK/BSI level, geometrical cross sections of 140.3 \AA^2 and 153.3 \AA^2 for Ar and Xe as target gases, respectively.

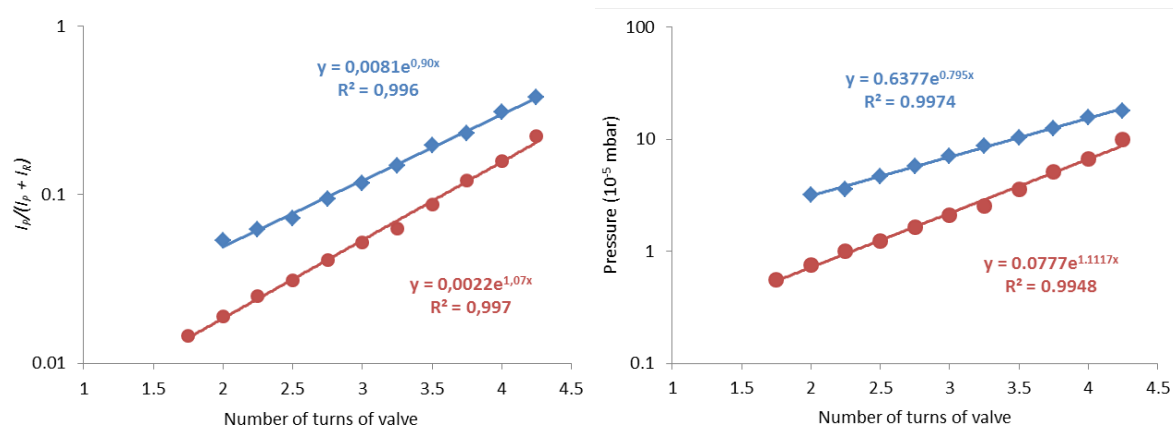


Figure S2. Product ion intensities as a function of number of turns of valve for collision-induced dissociation of $[\text{MePh}_2\text{PAu}]^+$ with collision on Ar (blue diamonds) and Xe (red circles) (left); Calibrations curves of the pressure as a function of number of turns of valve with Ar (blue) and Xe (Red) obtained using the fit of the data with *MassKinetics* software.

3. Geometrical collisional cross section calculations (S).

Van der Waals radii used for geometrical cross-section calculations: $R(\text{H}) = 1.10 \text{ \AA}$, $R(\text{C}) = 1.83 \text{ \AA}$, $R(\text{N}) = 1.70 \text{ \AA}$, $R(\text{O}) = 1.63 \text{ \AA}$, $R(\text{He}) = 1.09 \text{ \AA}$, $R(\text{Cl}) = 1.92 \text{ \AA}$, $R(\text{Ar}) = 1.88 \text{ \AA}$ and $R(\text{Xe}) = 2.16 \text{ \AA}$.

In order to confirm the validity of atomic parameters used, geometrical cross-sections (or hard spheres collision cross-section" (σ_{HS})) for pOMe **1**, pCl **3**, *tert*Bu ions were computed and compared with those obtained experimentally by Morsa & al. using a SYNAPT instrument with He injected inside the drift cell, respectively $93.7 \pm 1.9 \text{ \AA}^2$, $88.3 \pm 1.7 \text{ \AA}^2$ and $105.5 \pm 2.0 \text{ \AA}^2$. Results obtained with Batsanov's parameters ($91.5 \pm 5.5 \text{ \AA}^2$, $87.5 \pm 5.2 \text{ \AA}^2$, $101.1 \pm 6.1 \text{ \AA}^2$) slightly improved *S* values as compared with default atomic radii ($89.4 \pm 5.4 \text{ \AA}^2$, $84.2 \pm 5.0 \text{ \AA}^2$, $98.8 \pm 5.9 \text{ \AA}^2$). The same procedure was then used to obtain geometrical cross sections for all benzylpyridinium salts leading to the following values : with Argon as target gas $S_{\text{Ar}}(\text{pOMe } \mathbf{1}) = 122.9 \pm 7.4 \text{ \AA}^2$, $S_{\text{Ar}}(\text{pMe } \mathbf{2}) = 118.3 \pm 7.1 \text{ \AA}^2$, $S_{\text{Ar}}(\text{pCl } \mathbf{3}) = 118.1 \pm 7.1 \text{ \AA}^2$, $S_{\text{Ar}}(\text{pCN } \mathbf{4}) = 121.8 \pm 7.3 \text{ \AA}^2$ and with Xe as target gas $S_{\text{Xe}}(\text{pOCH}_3 \mathbf{1}) = 134.9 \pm 8.1 \text{ \AA}^2$, $S_{\text{Xe}}(\text{pMe } \mathbf{2}) = 130.2 \pm 7.8 \text{ \AA}^2$, $S_{\text{Xe}}(\text{pCl } \mathbf{3}) = 129.8 \pm 7.8 \text{ \AA}^2$, $S_{\text{Xe}}(\text{pCN } \mathbf{4}) = 133.7 \pm 8.0 \text{ \AA}^2$.

Default 2 % accuracy was used in the algorithm; calculations were repeated 500 times to obtain averaged values and standard deviations of 0.6 %. Error bars on reported geometrical cross sections were estimated with the following 3 components: $\pm 6 \%$ variation in the buffer gas radius led to approx. $\pm 3.3 \%$ in determined collisional cross section, 0.6 % from numerical errors and a rough estimate of 2 % from uncertainties in atomic parameters, the sum of which was rounded to 6 %.

4. Retarding potential analysis and Kinetic energy distribution of the precursor ion beam

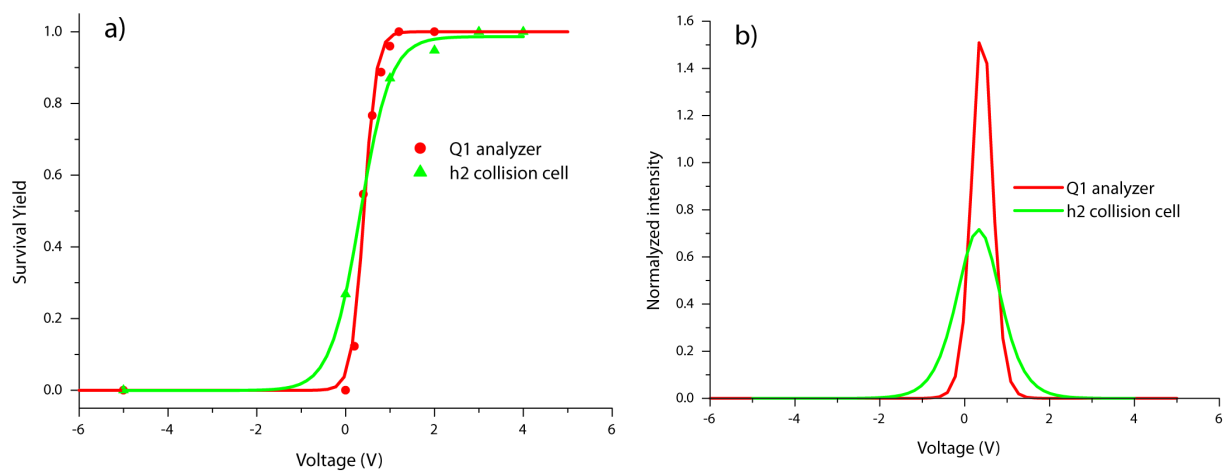


Figure S3. a) Retarding potential analysis performed in the Q1 analyzer and h2 hexapole. b) Derivative curves of the retarding potential analysis curves leading to the kinetic energy distributions of the precursor ion beam. The green curve represents a Gaussian fit characterized by a mean of 0.4 eV and FWHM of 1.2 eV in the h2 collision cell. The energy distribution measured in the first quadrupole (0.4 eV and FWHM of 0.6 eV) is also reported (red curve).

5. Effects of kinetic and internal energy distributions

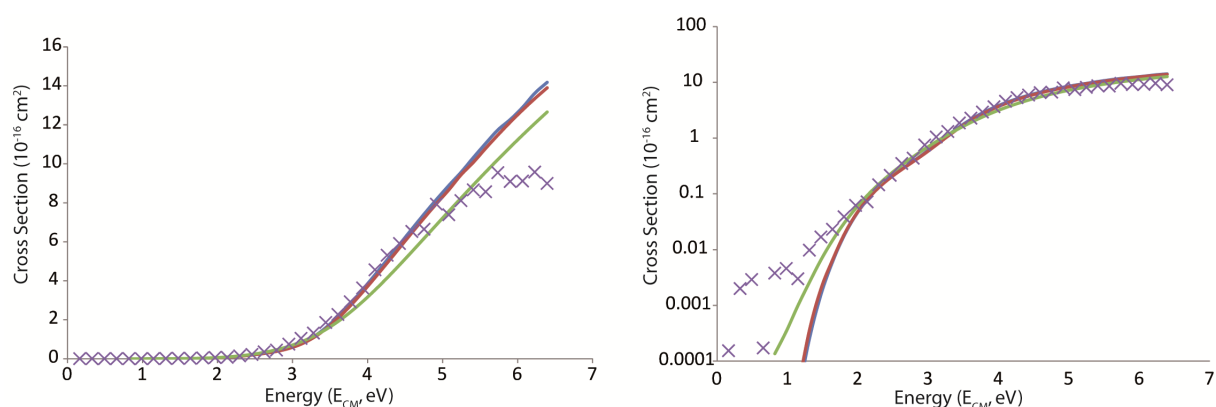


Figure S4. Comparison of the precursor ion abundances pCl 3 measured (velvet cross) and calculated for different initial kinetic and internal energies and for different critical energies used: $E_k=300$ K, $E_{int}=300$ K and $E_0=1.87$ eV (blue curve), $E_k=300$ K, $E_{int}=700$ K and $E_0=2.37$ eV (corresponding to a shift of 0.5 eV for the E_0 , as experimentally observed) (green curve), $E_k=5800$ K, $E_{int}=300$ K and $E_0=1.89$ eV (red line), (note that $E_k=5800$ K is close to a Gaussian curve characterized by a full width at half maximum of 1.3 eV and a shift of 0.5 eV, as experimentally observed).

6. $\log(k.s)$ and sum of states vs. bond elongation for different internal energies

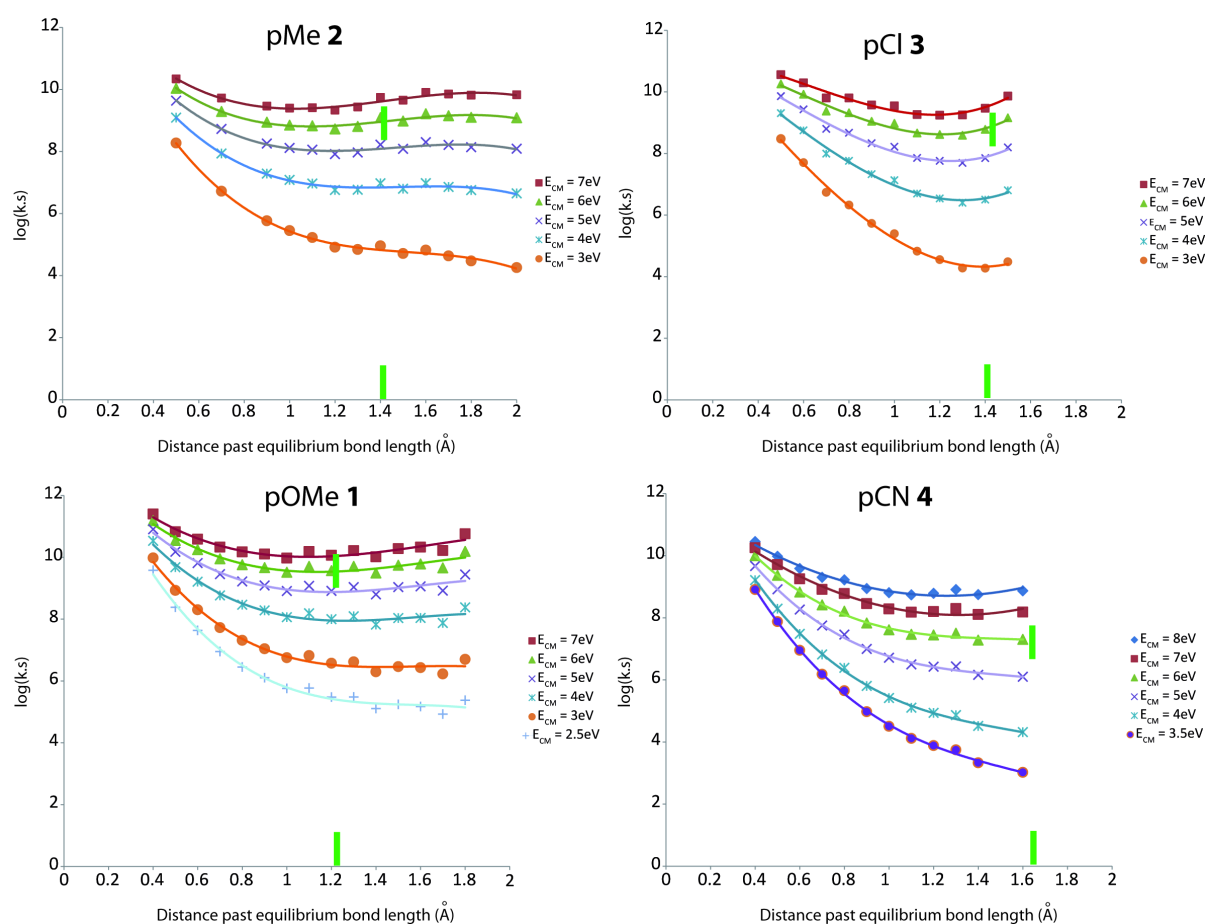


Figure S5. Plot for the four BP^+ ions showing the logarithm of the kinetic rate of decomposition calculated at each step along their fragmentation for different internal energies (E_0 and frequency models were calculated at BMK/BSI level). The green lines correspond to the minima of the sum of states calculated by DeBord et al.

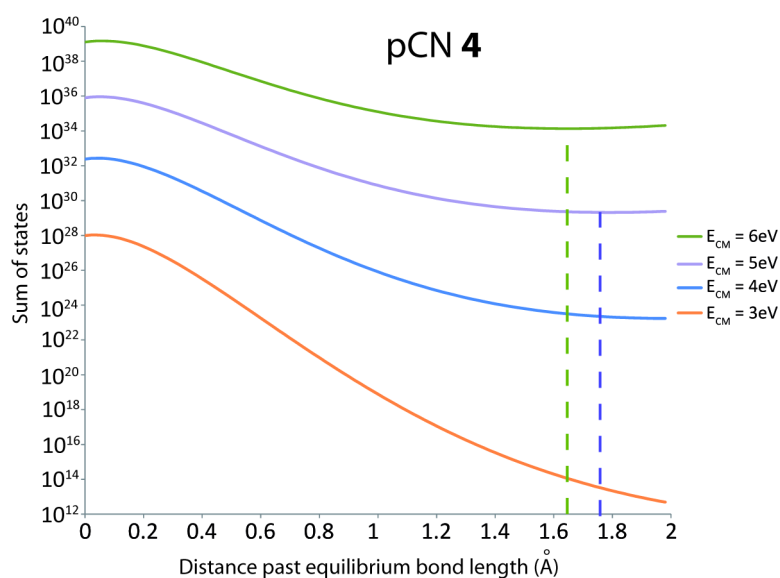


Figure S6. Plot for pCN 4 showing the sum of states calculated at each step along their fragmentation pathways at an internal energy range between 3 and 6 eV. The lines correspond to the minima of the sum of states. The code developed by Simon W. North (see for example *The Journal of Chemical Physics* 110, 2862 (1999); doi: 10.1063/1.477929 by Agnes Derecskei-Kovacs and Simon North) was used. The frequencies of the transitional modes were assumed to change smoothly with the distance of elongation R according to the formula: $\nu_{\text{tri}} = \nu_{\text{tri}}(R_e) \exp(-aR)$. The constant “a” was taken equal to 1.2. R_e is the equilibrium C-N bond distance.